Prediction of high-T_c superconductivity under submegabar pressure in ternary actinium borohydrides

Tingting Gu,[1] Wenwen Cui,[1,*] Jian Hao,[1] Jingming Shi,[1] Artur P. Durajski,[2] Hanyu Liu,[3,†] and Yinwei Li[1,‡]

[1]*Laboratory of Quantum Functional Materials Design and Application, School of Physics and Electronic Engineering, Jiangsu Normal University, Xuzhou 221116, China*

[2]*Institute of Physics, Częstochowa University of Technology, Avenue Armii Krajowej 19, 42-200 Częstochowa, Poland*

[3]*Key Laboratory of Material Simulation Methods and Software of Ministry of Education and State Key Laboratory of Superhard Materials, College of Physics, Jilin University, Changchun 130012, China*

(Received 23 May 2024; revised 6 August 2024; accepted 9 August 2024; published 23 August 2024)

Ternary hydrides are considered as the ideal candidates with high critical temperature (T_c) stabilized at submegabar pressure, evidenced by the recent discoveries in $LaBeH_8$ (110 K at 80 GPa) and LaB_2H_8 (106 K at 90 GPa). Here, we investigate the crystal structures and superconductivity of an Ac-B-H system under pressures of 100 and 200 GPa by using an advanced structure method combined with first-principles calculations. As a result, nine stable compounds were identified, where B atoms are bonded with H atoms in the formation with diverse BH_x motifs, e.g., methanelike (BH_4), polythenelike, $(BH_2)_n$, and BH_6 octahedron. Among them, seven Ac-B-H compounds were found to become superconductive. In particular, $AcBH_7$ was estimated to have a T_c of 122 K at 70 GPa. Our in-depth analysis reveals that the B-H interactions in the BH_6 units play a key role in its high superconductivity and stability at submegabar pressure. Our current results provide a guidance for future experiments to synthesize ternary hydride superconductors with high-T_c at moderate pressure.

DOI: 10.1103/PhysRevB.110.064105

I. INTRODUCTION

Hydrogen is considered as a promising candidate for high-temperature superconductors, due to its small atomic mass and strong phonon vibration frequency [1,2]. However, the metallization pressure required to compress hydrogen exceeds 450 GPa, which is difficult to achieve via current hydrostatic pressure experiments [3,4]. Ashcroft pioneered the possibility of finding high-temperature superconductors in hydrides because of the "chemical precompression" effect of non-hydrogen elements, which allows for the metallization of hydrides at lower pressures [5] than that for pure hydrogen. However, to search for a suitable hydride with high superconductivity remained a great challenge at that time. Until recent decades, owing to the rapid development of computational structure prediction algorithms, many hydrides were predicted to become stable at megabar pressures with high superconducting critical temperature above 200 K. These theoretical studies have led to a surge in the number of high-temperature superconductors synthesized in binary hydrides, e.g., H_3S [6–9], LaH_{10} [10–13], YH_6 [14–16], YH_9 [15,17], and CaH_6 [18–20].

Almost all possibilities have been theoretically explored for binary hydrides [21,22], thus it is highly desirable to explore ternary hydrides considering the addition of new elements and new configurations, which expands the material field to find structures in the ternary hydrides with higher T_c at relatively lower pressures. To date, increasing amounts of ternary hydrides have been synthesized experimentally with the high-temperature superconductivity: $(La, Y)H_{10}$ (253 K at 183 GPa) [23], $(La, Ce)H_9$ (178 K at 110 GPa or 176 K at 100 GPa) [24,25], $(La, Nd)H_{10}$ (148 K at 170 GPa) [26], and $(La, Al)H_{10}$ (223 K at 164 GPa) [27]. However, the pressure still exceeds 100 GPa beyond further application. Recently, research proposed an effective strategy to reduce the external pressure by adding a light element that binds with H atoms to form small molecules, acting as precompression factor, such as CH_4 in CSH_7 [28,29] and MC_2H_8 [30], B/BeH_8 in $X(B/Be)H_8$ [31–35], and BH_4 in XB_2H_8 [36,37]. In this way, the newly constructed structures could not only become stable at lower pressure but also remain good superconductivity. Recently, structures of Mg_2XH_6 type are proposed to be an ideal superconductor at ambient pressure, e.g., Mg_2IrH_6 ($T_c = 160$ K) [38,39]. Particularly, $LaBeH_8$ and LaB_2H_8 have been synthesized successfully below megabar pressure with T_c of 110 K at 80 GPa [34] and 106 K at 90 GPa [40], respectively, which greatly motivated us to hunt for high-T_c superconductors at moderate pressures in ternary hydrides.

The p^0 and d^1 metals with low-lying empty orbitals tend to form phonon-mediated high-T_c superconducting (HTSC) metal polyhydrides. Among them, actinium, which is similar to lanthanum in chemical properties, atomic size, electronegativity, and electronic configuration, forms many actinium hydrides with good superconducting properties: $R\bar{3}m$ AcH_{10} (251 K at 200 GPa), $I4/mmm$ AcH_{12} (173 K at 150 GPa), and $P\bar{6}m2$ AcH_{16} (241 K at 150 GPa) [41]. In addition, a large number of ternary borohydrides have been explored, e.g.,

*Contact author: wenwencui@jsnu.edu.cn
†Contact author: hanyuliu@jlu.edu.cn
‡Contact author: yinwei_li@jsnu.edu.cn

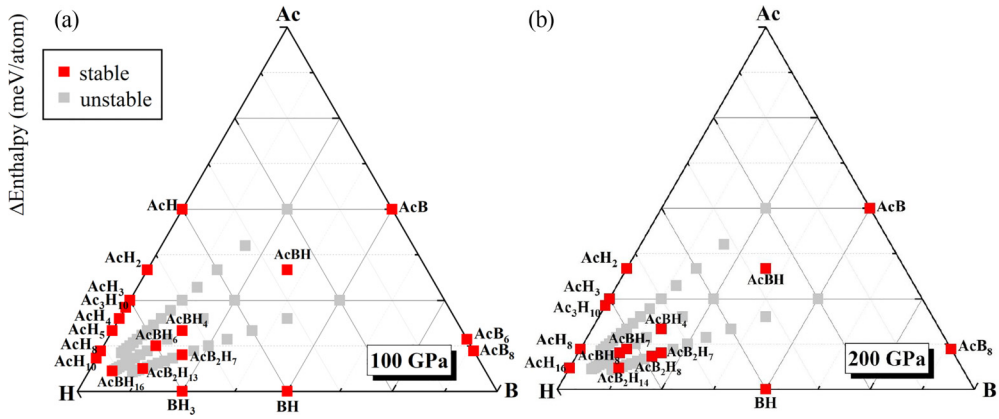

FIG. 1. Calculated stabilities of $Ac_xB_yH_z$ relative to Ac, B, H, and binary compounds at (a) 100 GPa and (b) 200 GPa. Red and gray squares denote the thermodynamically stable and ternary stoichiometries, respectively.

Li-B-H [42], S-B-H [43], Ca-B-H [44], Na-B-H [45], Mg-B-H [46], and La-B-H in particular, with a T_c of 126 K at 50 GPa [31–33]. On the basis, it is highly required to explore the crystal structure and superconductivity of the Ac-B-H system in anticipation of finding high-temperature superconductors stabilized at low pressures. In this work, the crystal structure, stability, and superconducting properties of $Ac_xB_yH_z$ ($x = 1$–2, $y = 1$–2, $z = 1$–16) at 100 and 200 GPa are theoretically investigated. Nine thermodynamically stable compounds are uncovered, namely, $P6/mmm$ AcBH, $P2_1/m$ $AcBH_4$, $P2_1/m$ AcB_2H_7, $Pbnm$ $AcBH_6$, $Pnm2_1$ AcB_2H_{14}, $Pm2_1b$ AcB_2H_{13}, $Pm2_1b$ $AcBH_{16}$, $P\bar{3}m1$ $AcBH_7$, and $P2_1/m$ $AcBH_8$. In particularly, $P\bar{3}m1$ $AcBH_7$ remains dynamically stable at 70 GPa with T_c of 122 K, comparable to that of $LaBeH_8$ (110 K at 80 GPa) [34] and LaB_2H_8 (106 K at 90 GPa) [40], which have already been synthesized experimentally.

II. COMPUTATIONAL DETAILS

The candidate structures of Ac-B and Ac-B-H systems are predicted using the CALYPSO code [47–50] based on a particle swarm optimization algorithm. We perform composition crystal structure searches for Ac_xB_y ($x = 1$–2, $y = 1$–10) and $Ac_xB_yH_z$ ($x = 1$–2, $y = 1$–2, $z = 1$–16) ranging from 1 to 4 f.u./cell at 100 and 200 GPa. More than 2000 structures for each stoichiometry during the prediction search and continues to generate 1000 structures after the lowest-energy structure is determined in order to ensure the convergence. The phonon calculations were performed for all structures by using a supercell method as implemented in the PHONOPY code [51,52]. The total energy and electronic properties are calculated by using the Vienna *ab initio* simulation package (VASP) [53] with the Perdew-Burke-Ernzerhof [54,55] exchange-correlation functional. Projector augmented-wave (PAW) potentials with the valence electrons $6s^26p^66d^17s^2$ for Ac, $5s^26s^25p^65d^1$ for La, $5s^26s^25p^65d^14f^1$ for Ce, $5s^26s^25p^65d^14f^1$ for Th, $2s^22p^1$ for B, and $1s^1$ for H are adopted [56]. To ensure the convergence of force and energy, we set the corresponding plane-wave cutoff energy to 600 eV and Brillouin zone samplings to 0.20 $Å^{-1}$. To consider the chemical bonding state of the structure, we have used the electron localization function (ELF) to analyze the covalent bonds and Bader to analyze the charge transfer [57,58]. The electron-phonon coupling (EPC) constant was calculated within the framework of the linear-response theory as carried out in the QUANTUM ESPRESSO package [59]. Ultrasoft pseudopotentials were used with a kinetic energy cutoff of 80 Ry. The detailed k meshes, and q points for superconducting Ac-B-H compounds can be found in the Supplemental Material (SM) [60]. Both EPC parameters and T_c calculated in the Ac-B-H system are based on the broadening parameter of 0.04 Ry. The Allen-Dynes modified McMillan (ADM) equation [61], which better describes superconductors with $\lambda < 1.5$, is applied in calculating it,

$$T_c = \frac{\omega_{\log}}{1.2} \exp\left[-\frac{1.04(1+\lambda)}{\lambda - \mu^*(1+0.62\lambda)}\right], \quad (1)$$

where $\omega_{\log}$ is the logarithmic average frequency, λ is the electron phonon coupling parameter, and μ^* is the Coulomb pseudopotential, often assumed to be between 0.1 and 0.13.

III. RESULTS AND DISCUSSION

In order to acquire the phase diagram of ternary Ac-B-H system, we need to first determine the structures of the associated binary system. The B-H system [62–67] and the Ac-H system [41] have been thoroughly investigated, while the information of the Ac-B system is lacking. Thus we make a structural prediction for Ac-B at pressures of 100 and 200 GPa and identified three thermodynamically stable compounds, namely, $R\bar{3}m$ AcB, $Pm\bar{3}m$ AcB_6, and $R\bar{3}m$ AcB_8 (see Figs. S1– S5 in SM [60] for more details). The calculated phase diagram of $Ac_xB_yH_z$ at pressures of 100 and 200 GPa is shown in Fig. 1. Six compounds are identified to be thermodynamically stable at 100 GPa (e.g., $P6/mmm$ AcBH, $P2_1/m$ $AcBH_4$, $Pbnm$ $AcBH_6$, $Pm2_1b$ $AcBH_{16}$, $P2_1/m$ AcB_2H_7, $Pm2_1b$ AcB_2H_{13}). Three compounds AcBH, $AcBH_4$, and AcB_2H_7 remain thermodynamically stable without phase transitions as pressure increases to 200 GPa. Additionally, another four stoichiometries $AcBH_7$, $AcBH_8$, AcB_2H_8, and AcB_2H_{14} start to locate at the convex hull at 200 GPa. Note that $AcBH_4$, $AcBH_6$, $AcBH_8$, and AcB_2H_8 have been reported in previous work [68], however, our proposed structures are more energetically stable with the exception of AcB_2H_8 which adopts the same symmetry $I4/mmm$ (see Fig. S6).

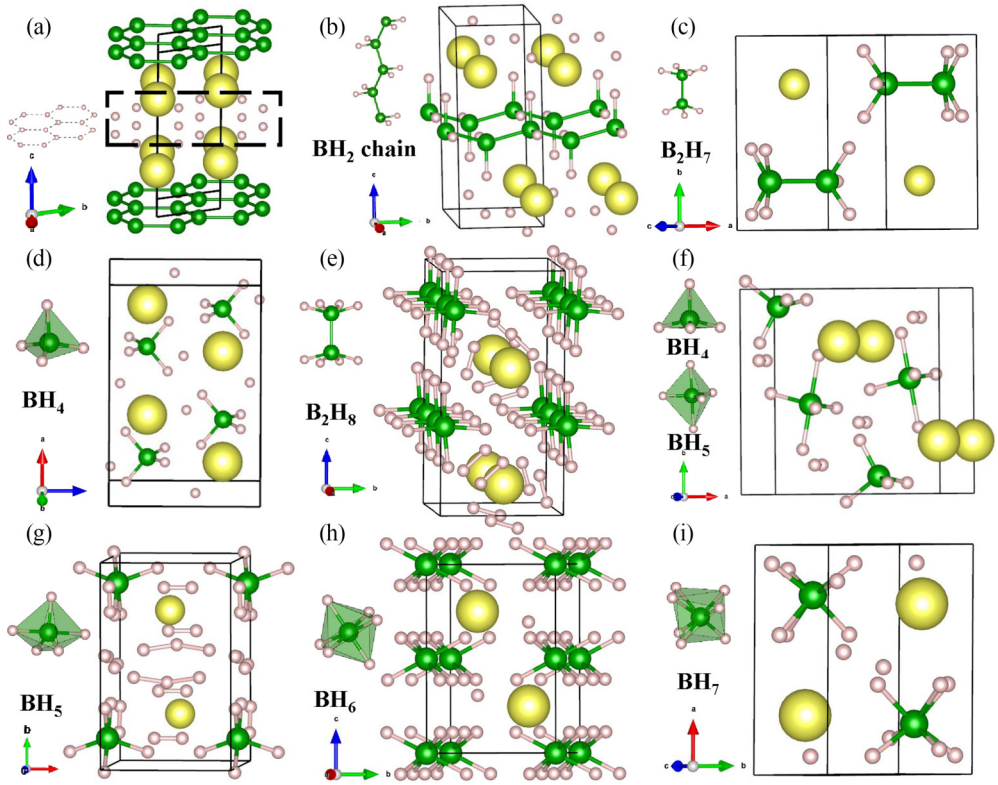

FIG. 2. The stable structures of Ac-B-H compounds: (a) $P6/mmm$ AcBH, (b) $P2_1/m$ $AcBH_4$, (c) $P2_1/m$ AcB_2H_7, (d) $Pnm2_1$ AcB_2H_{14}, (e) $Pbnm$ $AcBH_6$, (f) $Pm2_1b$ AcB_2H_{13}, (g) $Pm2_1b$ $AcBH_{16}$, (h) $P\bar{3}m1$ $AcBH_7$, and (i) $P2_1/m$ $AcBH_8$. Yellow, green, and pink spheres represent Ac, B, and H atoms, respectively.

Figure 2 shows the structures of nine Ac-B-H compounds with corresponding structural parameters as indicated in SM [60]. AcBH adopts hexagonal $P6/mmm$ symmetry, comprising alternating Ac, B, and H layers, where B and H atoms form the honeycomb sublattice [Fig. 2(a)]. In $AcBH_4$ [Fig. 2(b)], the zigzag B covalently bonded with two hydrogen atoms to form BH_2 units, which are polymerized along the y axis and behave as polythene. For H-richer AcB_2H_7 [Fig. 2(c)], it consists of Ac atoms and B_2H_7 units, where the bond length between B-B is 1.58 Å at 100 GPa, and it is strongly covalently bonded with the ends coordinated to three H atoms and four H atoms. Interestingly, AcB_2H_{14} contains B_2H_8 units, composed of two BH_4 linked by B-B covalent bonds, while three H_2 molecules in the same plane surround Ac atoms [Fig. 2(d)]. With increasing H contents, BH_4, BH_5, BH_6, and BH_7 appears in $AcBH_6$, AcB_2H_{13}, $AcBH_{16}$, $AcBH_7$, and $AcBH_8$, respectively [Figs. 2(e)–2(i)]. In particular, $AcBH_7$ adopts high-symmetry $P\bar{3}m1$ [Fig. 2(h)], isostructural with $LaBH_7$ [32]. The BH_6 units locate at the vertices and edges of the hexagonal lattice, and the ones on the edges are connected by H atoms. In addition to BH_x units, the extra H atoms in the Ac-B-H compounds exist in many forms, e.g., monoatomic H (e.g., $AcBH_4$, AcB_2H_7, $AcBH_6$, AcB_2H_8, AcB_2H_{14}, AcB_2H_{13}, $AcBH_{16}$, $AcBH_7$, $AcBH_8$), H_2 (e.g., AcB_2H_8, AcB_2H_{14}, AcB_2H_{13}, $AcBH_{16}$), and linear H_3 (e.g., $AcBH_{16}$).

In order to further explore the fascinating properties of Ac-B-H compounds, we calculated their electronic structure and phonon properties. Almost all the predicted structures are metallic with several bands crossing the Fermi energy level, with the exception of $AcBH_6$ and AcB_2H_7, both of which are semiconductors (see Fig. 3 and Figs. S8 and S9). The significant overlap of the partial electronic density of states (DOS) of the different atoms indicates a strong hybridization of Ac-H and B-H under pressure. Note that T_c in BCS theory is closely related to the DOS of E_f. Additionally, the occupation of H at E_f (DOS_H) plays a crucial role as well. For the metallic structures, hydrogen atoms make a substantial contribution to the total DOS of E_f, e.g., for $AcBH_{16}$ (68%), AcB_2H_{13}(64%), $AcBH_7$(48%), $AcBH_8$ (53%), AcB_2H_8 (54%), and AcB_2H_{14} (58%) (see Table S2). Considering these two criteria, five stable metallics of Ac-B-H compounds are screened as the potential superconductors: AcB_2H_8, AcB_2H_{14}, $AcBH_{16}$, $AcBH_7$, and $AcBH_8$.

Based on the metallic properties of Ac-B-H compounds, we calculated their phonon dispersions, projected phonon DOS (PHDOS), Eliashberg spectral function $\alpha^2F(\omega)$, and EPC integral $\lambda(\omega)$ at 200 GPa as shown in Fig. 4 and Figs. S10–S12. The phonon dispersion supports their dynamical stability via the absence of any imaginary frequencies. Furthermore, the dynamical stabilities of $LaBH_7$ (at 85 GPa), $AcBH_7$ (at 70 GPa), and AcB_2H_8 (at 125 GPa) are confirmed by calculating PHDOS with larger q meshes (Fig. S13). The common feature of the phonons is that the lowest-frequency vibrational modes are contributed by the heavy atoms Ac, B, and H dominate the midfrequency modes, and the high-frequency modes are exclusively from H atoms. The superconducting properties were then evaluated using the

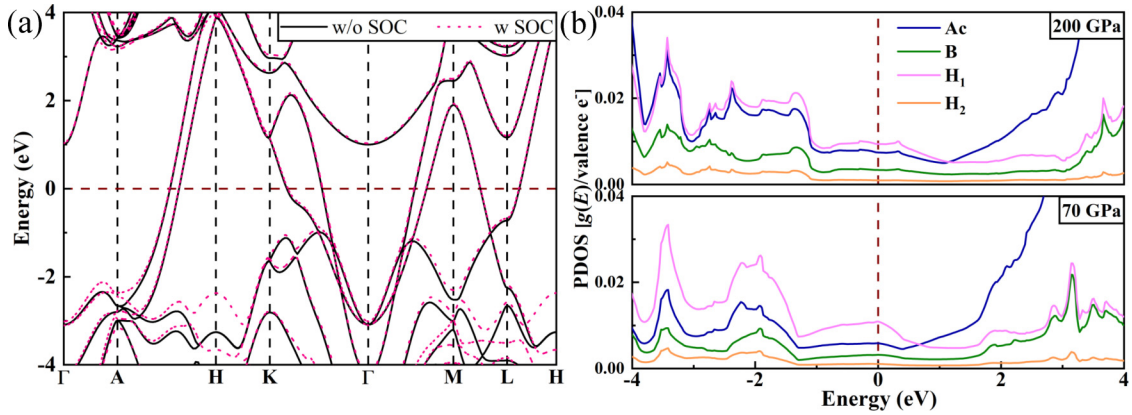

FIG. 3. (a) Electronic band structures of $P\bar{3}m1$ $AcBH_7$ at 200 GPa without ("w/o SOC") and with the inclusion of spin-orbit coupling ("w SOC"). The Fermi energy is set to zero. (b) Atom-projected density of states near the Fermi level for $P\bar{3}m1$ $AcBH_7$ at 200 and 70 GPa. H_1 denotes the H atoms in the BH_6 units, and H_2 denotes the H atom that is not bonded to the B atom.

Allen-Dynes-modified McMillan equation [61] or by solving numerically the Eliashberg equations [69]. We used the typical value of the Coulomb pseudopotential $\mu^\star = 0.10$. The results are summarized in Table I.

AcB_2H_8 exhibits good superconductivity with T_c above 70 K at 200 GPa (Fig. S12). As the pressure decreases to 125 GPa, the superconductivity is almost unchanged with 79 K, which agrees well with the previous work [68]. Other compounds possess the similar superconductivity with T_c around 40 K at the corresponding predicted pressure. $AcBH_{16}$ and AcB_2H_{14} are dynamically unstable below 90 and 180 GPa, respectively, thus their electronic properties are excluded from consideration at low pressure. Additionally, AcB_2H_8 has been reported previously, thus hereafter our calculations and discussions will focus on $AcBH_8$ and $AcBH_7$, which could remain dynamically stable at lower pressure.

By further inspection, they have the close DOS at E_f and DOS_H contribution at 200 GPa for $AcBH_8$ (0.030 eV^{-1} per valence electron, 53% from DOS_H) [Fig. S9(a)] and $AcBH_7$ (0.028 eV^{-1} per valence electron, 48% from DOS_H) [Fig. 3(b)]. Consequently, they exhibit very similar superconductivity. As the pressure decreases to 100 GPa, both the DOS at E_f and H contribution in $AcBH_8$ decrease accordingly (Table S2). Additionally, the phonons show obvious softening at high frequencies under decompression (Fig. S10), which leads to an increase in the EPC parameter λ from 0.64 to 0.71, while the average phonon frequency ω_{log} decreases

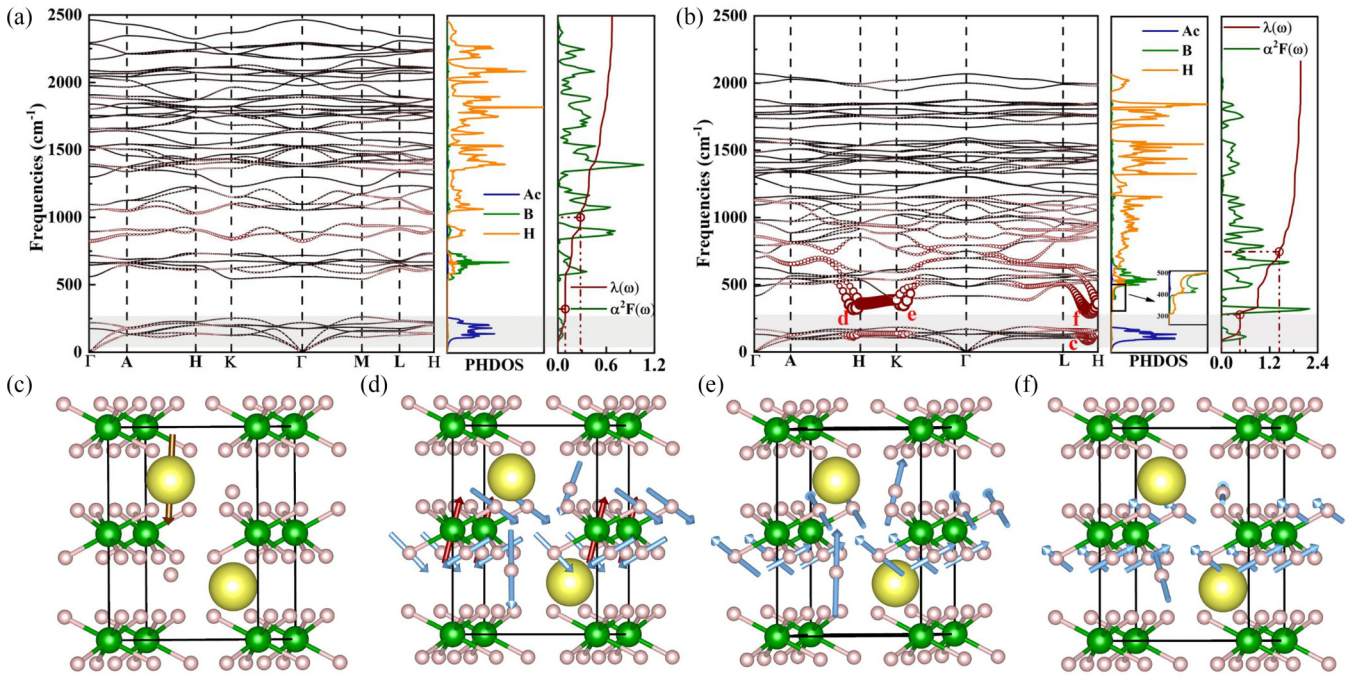

FIG. 4. Phonon-dispersion curves, PHDOS, projected on the Ac, B, and H atoms, Eliashberg spectral function, $\alpha^2F(\omega)$ and $\lambda(\omega)$ for $P\bar{3}m1$ $AcBH_7$ at (a) 200 GPa and (b) 70 GPa. (c)–(f) The vibrational modes at c, d, e, and f of $P\bar{3}m1$ $AcBH_7$ at 70 GPa. The direction of vibration of Ac, B, and H are marked as golden, red, and blue arrows, respectively.

TABLE I. The calculated electron-phonon coupling parameter (λ), logarithmic average phonon frequency ω_{log}, and the estimated T_c for $Pm2_1b$ $AcBH_{16}$, $P\bar{3}m1$ $AcBH_7$, $P2_1/m$ $AcBH_8$, $Pm2_1b$ AcB_2H_{13}, and $Pnm2_1$ AcB_2H_{14} at high pressures.

Phases	Pressure (GPa)	λ	ω_{log} (K)	T_c (K) ADM	T_c (K) Eliashberg
$Pm2_1b$ $AcBH_{16}$	100	0.71	950.77	35	39
$P\bar{3}m1$ $AcBH_7$	200	0.67	1309.04	41	43
	70	1.98	600.86	86	122
$P2_1/m$ $AcBH_8$	200	0.64	1368.91	37	43
	100	0.71	1118.08	40	46
$Pnm2_1$ AcB_2H_{14}	200	0.72	1108.48	41	42

from 1368 to 1118 K, leading to the combined effect of a slight increase in T_c from 43 K at 200 GPa to 46 K at 100 GPa.

For $AcBH_7$, there are two bands crossing the Fermi energy level at 200 GPa with the largest contribution from H atoms to the total DOS [Figs. 3(a) and 3(b)]. When the pressure decreases to 70 GPa, the total DOS increases to 0.037 eV^{-1} per valence electron, accompanied by an increase in DOS_H contribution [56%, Fig. 3(b)], indicating the greater possibility to form the Cooper pairs that may contribute to higher T_c. We further investigate the spin-orbit coupling (SOC) effect on the band structures of Ac-B-H compounds [Fig. 3(a) and Figs. S8 and S9], and found that they are nearly identical, indicating that the band structures are insensitive to SOC for actinium borohydrides. The calculated λ and ω_{log} are 0.67 and 1309.04 K at 200 GPa, respectively, leading to a T_c of 43 K. The low (0–250 cm^{-1}), mid (500–1000 cm^{-1}), and high frequencies (1000–2500 cm^{-1}) contribute 13%, 28%, and 59% to the λ, respectively [Fig. 4(a)]. As the pressure is lowered to 70 GPa, λ increases to 1.98, with a T_c of 122 K. The enhanced superconductivity mainly originates from four softened modes labeled as *c*, *d*, *e*, and *f*. Among these, the contribution of low frequency (0–250 cm^{-1}) induced by Ac atoms increases to 23% to the total λ, due to the soft modes along L-H at site *c* [Fig. 4(b)]. More interestingly, the interaction between B and H becomes stronger, and the midfrequency contribution to λ due to soft phonon modes at *d*, *e*, and *f* (250–750 cm^{-1}) increases to 48%. The detailed vibration modes of four soft modes at Fig. 4(b) are shown in Figs. 4(c)–4(f). Specifically, the heavy Ac atoms contribute to the low-frequency modes at the *c* site. For the *e* and *f* sites, the softened vibrations modes are mainly originated from H atoms [Figs. 4(e) and 4(f)], while at the *d* and *e* sites, the combined effect of B and H vibrations plays a key role in the phonon softening [see Fig. 4(d)].

As compared with $AcBH_7$, isostructural $LaBH_7$ is calculated to remain dynamical stable at higher pressure (85 GPa), due to the smaller atomic mass of La atoms, which reduces the chemical precompression on BH_6 units. This is evidenced by comparing the lattice constant and B-H bond length in $LaBH_7$ and $AcBH_7$ (Fig. S14). The substitution of La atoms results in an increase in the lattice constants a (=b), from 3.79 Å in $AcBH_7$ (70 GPa) to 3.91 Å (85 GPa) in $LaBH_7$, which is more obvious in the *c* direction, from 5.21 to 5.75 Å.

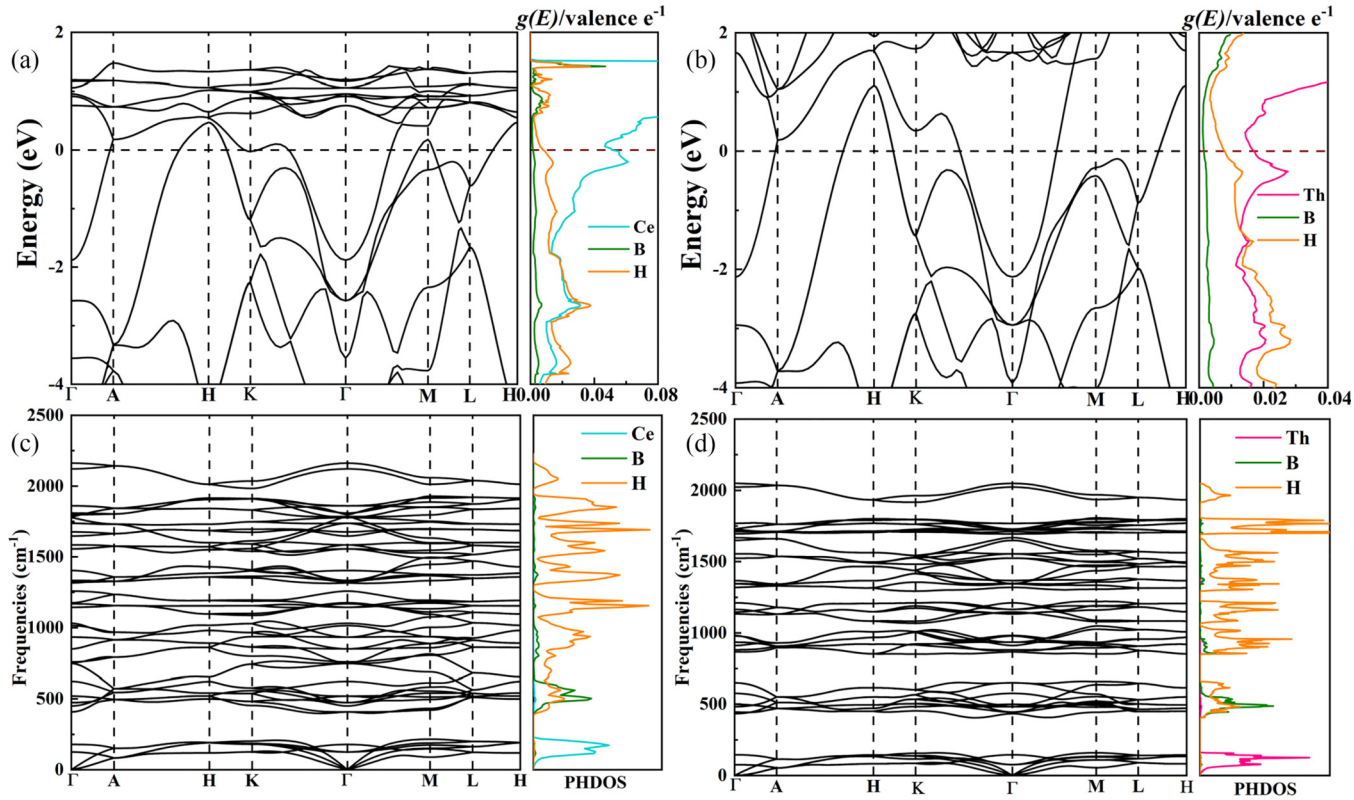

FIG. 5. The projected electronic band structure of each atoms in (a) $CeBH_7$ at 75 GPa and (b) $ThBH_7$ at 50 GPa. Phonon-dispersion curves, phonon density of states (PHDOS) for (c) $CeBH_7$ at 75 GPa and (d) $ThBH_7$ at 50 GPa.

Correspondingly, the length of the B-H bond in $AcBH_7$ is slightly shorter (~0.05 Å) than that in $LaBH_7$. Although the electron occupation at E_f in $LaBH_7$ at 85 GPa (0.043 eV^{-1} per valence electron) is larger than that of $AcBH_7$ (0.037 eV^{-1} per valence electron) at 70 GPa. The contribution of H atoms is smaller with only 44% [Fig. S15(a)], leading to the same DOS_H at E_f with that of $AcBH_7$. Additionally, $LaBH_7$ has the same λ (1.98), which is originated mainly from the contributions of B and H atoms at low and midfrequencies (55%) [Fig. S15(b)]. Consequently, they exhibit the same superconductivity with $T_c$of 120 K (Table S3).

The effect of metal atoms on the superconductivity of this structure is further investigated by substituting the Ac atoms with its neighboring metal atoms Th and Ce. Note that the space group $P\bar{3}m1$ evolves to $P6_3/mmc$ after full optimization. The superconducting parameters of $CeBH_7$ and $ThBH_7$ at their lowest dynamically stable pressures were summarized in Table S3. The onset pressure of dynamical stability for $CeBH_7$ (75 GPa) and $ThBH_7$ (50 GPa) is reduced compared to that of $LaBH_7$ and $AcBH_7$. It is reasonable considering the stronger chemical compression from their larger atomic masses. However, their superconductivity is significantly weakened, only 18 and 51 K for $CeBH_7$ and $ThBH_7$, respectively. By comparing their electronic properties [Figs. 5(a) and 5(b)], we find that both $ThBH_7$ and $CeBH_7$ have larger total DOS at E_f, however, the contribution of H atoms to the DOS is much smaller in the metal atoms Ce and Th. This is obviously not favorable to obtain good superconductivity. Thus their phonons display very similar features, which are also divided into three parts, but with much smaller λ, 0.61 and 1.04 for $CeBH_7$ and $ThBH_7$, respectively [Figs. 5(c) and 5(d) and Fig. S16]. These results further demonstrate the key role of H-dominated DOS at E_f in attaining high-T_c superconductors.

IV. CONCLUSIONS

In summary, the crystal structure and superconductivity of the Ac-B-H system at 100 and 200 GPa are explored by a combination of structure prediction methods and first-principles calculations. We uncover nine thermodynamically stable structures, namely, AcBH, $AcBH_4$, $AcBH_6$, $AcBH_{16}$, AcB_2H_7, AcB_2H_{13}, $AcBH_7$, $AcBH_8$, and AcB_2H_{14}. Seven of them exhibit a metallic nature. Electron-phonon coupling calculations show that $AcBH_7$ is a potential superconductor with T_c of 43 K at 200 GPa. Interestingly, it remains dynamically stable down to 70 GPa with an increased T_c of 122 K. The enhanced superconductivity is mainly attributed to the softened phonon vibrations originating from Ac atoms at low frequency, as well as B-H interactions in BH_6 units at midfrequency. Our work is expected to stimulate more research on ternary superconducting hydrides in the hope to uncover more compounds with high critical temperature and stability at low pressure.

ACKNOWLEDGMENTS

The authors acknowledge funding from the NSFC under Grants No. 12074154, No. 12174160, No. 12074138, No. 52288102, No. 52090024, and No. 11722433. Y.L. acknowledges the funding from the Six Talent Peaks Project and 333 High-level Talents Project of Jiangsu Province. H.L. acknowledges the funding from the Strategic Priority Research Program of Chinese Academy of Sciences (Grant No. XDB33000000). A.P.D. is grateful for financial support from the National Science Centre (Poland) through Project No. 2022/47/B/ST3/00622. All the calculations were performed at the High Performance Computing Center of the School of Physics and Electronic Engineering of Jiangsu Normal University.

[1] E. Wigner and H. B. Huntington, On the possibility of a metallic modification of hydrogen, J. Chem. Phys. **3**, 764 (1935).

[2] N. W. Ashcroft, Metallic hydrogen: A high-temperature superconductor? Phys. Rev. Lett. **21**, 1748 (1968).

[3] S. Azadi, B. Monserrat, W. M. C. Foulkes, and R. J. Needs, Dissociation of high-pressure solid molecular hydrogen: A quantum Monte Carlo and anharmonic vibrational study, Phys. Rev. Lett. **112**, 165501 (2014).

[4] J. McMinis, R. C. Clay III, D. Lee, and M. A. Morales, Molecular to atomic phase transition in hydrogen under high pressure, Phys. Rev. Lett. **114**, 105305 (2015).

[5] N. W. Ashcroft, Hydrogen dominant metallic alloys: High temperature superconductors? Phys. Rev. Lett. **92**, 187002 (2004).

[6] Y. Li, J. Hao, H. Liu, Y. Li, and Y. Ma, The metallization and superconductivity of dense hydrogen sulfide, J. Chem. Phys. **140**, 174712 (2014).

[7] D. Duan, X. Huang, F. Tian, D. Li, H. Yu, Y. Liu, Y. Ma, B. Liu, and T. Cui, Pressure-induced decomposition of solid hydrogen sulfide, Phys. Rev. B **91**, 180502(R) (2015).

[8] D. Duan, Y. Liu, F. Tian, D. Li, X. Huang, Z. Zhao, H. Yu, B. Liu, W. Tian, and T. Cui, Pressure-induced metallization of dense $(H_2S)_2H_2$ with high-T_c superconductivity, Sci. Rep. **4**6968 (2014).

[9] A. Drozdov, M. Eremets, I. Troyan, V. Ksenofontov, and S. I. Shylin, Conventional superconductivity at 203 Kelvin at high pressures in the sulfur hydride system, Nature (London) **525**, 73 (2015).

[10] H. Liu, I. I. Naumov, R. Hoffmann, N. Ashcroft, and R. J. Hemley, Potential high-T_c superconducting lanthanum and yttrium hydrides at high pressure, Proc. Natl. Acad. Sci. USA **114**, 6990 (2017).

[11] A. Drozdov, P. Kong, V. Minkov, S. Besedin, M. Kuzovnikov, S. Mozaffari, L. Balicas, F. Balakirev, D. Graf, V. Prakapenka *et al.*, Superconductivity at 250 K in lanthanum hydride under high pressures, Nature (London) **569**, 528 (2019).

[12] F. Peng, Y. Sun, C. J. Pickard, R. J. Needs, Q. Wu, and Y. Ma, Hydrogen clathrate structures in rare earth hydrides at high pressures: Possible route to room-temperature superconductivity, Phys. Rev. Lett. **119**, 107001 (2017).

[13] M. Somayazulu, M. Ahart, A. K. Mishra, Z. M. Geballe, M. Baldini, Y. Meng, V. V. Struzhkin, and R. J. Hemley, Evidence for superconductivity above 260 K in lanthanum superhydride at megabar pressures, Phys. Rev. Lett. **122**, 027001 (2019).

[14] Y. Li, J. Hao, H. Liu, J. S. Tse, Y. Wang, and Y. Ma, Pressure-stabilized superconductive yttrium hydrides, Sci. Rep. **5**, 9948 (2015).

[15] P. Kong, V. S. Minkov, M. A. Kuzovnikov, A. P. Drozdov, S. P. Besedin, S. Mozaffari, L. Balicas, F. F. Balakirev, V. B. Prakapenka, S. Chariton *et al.*, Superconductivity up to 243 K in the yttrium-hydrogen system under high pressure, Nat. Commun. **12**, 5075 (2021).

[16] I. A. Troyan, D. V. Semenok, A. G. Kvashnin, A. V. Sadakov, O. A. Sobolevskiy, V. M. Pudalov, A. G. Ivanova, V. B. Prakapenka, E. Greenberg, A. G. Gavriliuk *et al.*, Anomalous high-temperature superconductivity in YH_6, Adv. Mater. **33**, 2006832 (2021).

[17] E. Snider, N. Dasenbrock-Gammon, R. McBride, X. Wang, N. Meyers, K. V. Lawler, E. Zurek, A. Salamat, and R. P. Dias, Synthesis of yttrium superhydride superconductor with a transition temperature up to 262 K by catalytic hydrogenation at high pressures, Phys. Rev. Lett. **126**, 117003 (2021).

[18] H. Wang, J. S. Tse, K. Tanaka, T. Iitaka, and Y. Ma, Superconductive sodalite-like clathrate calcium hydride at high pressures, Proc. Natl. Acad. Sci. U.S.A. **109**, 6463 (2012).

[19] L. Ma, K. Wang, Y. Xie, X. Yang, Y. Wang, M. Zhou, H. Liu, X. Yu, Y. Zhao, H. Wang *et al.*, High-temperature superconducting phase in clathrate calcium hydride CaH_6 up to 215 K at a pressure of 172 GPa, Phys. Rev. Lett. **128**, 167001 (2022).

[20] Z. Li, X. He, C. Zhang, X. Wang, S. Zhang, Y. Jia, S. Feng, K. Lu, J. Zhao, J. Zhang *et al.*, Superconductivity above 200 K discovered in superhydrides of calcium, Nat. Commun. **13**, 2863 (2022).

[21] E. Zurek and T. Bi, High-temperature superconductivity in alkaline and rare earth polyhydrides at high pressure: A theoretical perspective, J. Chem. Phys. **150**, 050901 (2019).

[22] J. A. Flores-Livas, L. Boeri, A. Sanna, G. Profeta, R. Arita, and M. Eremets, A perspective on conventional high-temperature superconductors at high pressure: Methods and materials, Phys. Rep. **856**, 1 (2020).

[23] D. V. Semenok, I. A. Troyan, A. G. Ivanova, A. G. Kvashnin, I. A. Kruglov, M. Hanfland, A. V. Sadakov, O. A. Sobolevskiy, K. S. Pervakov, I. S. Lyubutin *et al.*, Superconductivity at 253 K in lanthanum–yttrium ternary hydrides, Mater. Today **48**, 18 (2021).

[24] W. Chen, X. Huang, D. V. Semenok, S. Chen, D. Zhou, K. Zhang, A. R. Oganov, and T. Cui, Enhancement of superconducting properties in the La–Ce–H system at moderate pressures, Nat. Commun. **14**, 2660 (2023).

[25] J. Bi, Y. Nakamoto, P. Zhang, K. Shimizu, B. Zou, H. Liu, M. Zhou, G. Liu, H. Wang, and Y. Ma, Giant enhancement of superconducting critical temperature in substitutional alloy $(La,Ce)H_9$, Nat. Commun. **13**, 5952 (2022).

[26] D. V. Semenok, I. A. Troyan, A. V. Sadakov, D. Zhou, M. Galasso, A. G. Kvashnin, A. G. Ivanova, I. A. Kruglov, A. A. Bykov, K. Y. Terent'ev *et al.*, Effect of magnetic impurities on superconductivity in LaH_{10}, Adv. Mater. **34**, 2204038 (2022).

[27] S. Chen, Y. Qian, X. Huang, W. Chen, J. Guo, K. Zhang, J. Zhang, H. Yuan, and T. Cui, High-temperature superconductivity up to 223 K in the Al stabilized metastable hexagonal lanthanum superhydride, Natl. Sci. Rev. **11**, nwad107 (2024).

[28] W. Cui, T. Bi, J. Shi, Y. Li, H. Liu, E. Zurek, and R. J. Hemley, Route to high-T_c superconductivity via CH_4-intercalated H_3S hydride perovskites, Phys. Rev. B **101**, 134504 (2020).

[29] Y. Sun, Y. Tian, B. Jiang, X. Li, H. Li, T. Iitaka, X. Zhong, and Y. Xie, Computational discovery of a dynamically stable cubic SH_3-like high-temperature superconductor at 100 GPa via CH_4 intercalation, Phys. Rev. B **101**, 174102 (2020).

[30] M.-J. Jiang, Y.-L. Hai, H.-L. Tian, H.-B. Ding, Y.-J. Feng, C.-L. Yang, X.-J. Chen, and G.-H. Zhong, High-temperature superconductivity below 100 GPa in ternary C-based hydride MC_2H_8 with molecular crystal characteristics (M = Na, K, Mg, Al, and Ga), Phys. Rev. B **105**, 104511 (2022).

[31] S. Di Cataldo, C. Heil, W. von der Linden, and L. Boeri, $LaBH_8$: Towards high-T_c low-pressure superconductivity in ternary superhydrides, Phys. Rev. B **104**, L020511 (2021).

[32] X. Liang, A. Bergara, X. Wei, X. Song, L. Wang, R. Sun, H. Liu, R. J. Hemley, L. Wang, G. Gao *et al.*, Prediction of high-T_c superconductivity in ternary lanthanum borohydrides, Phys. Rev. B **104**, 134501 (2021).

[33] F. Belli and I. Errea, Impact of ionic quantum fluctuations on the thermodynamic stability and superconductivity of $LaBH_8$, Phys. Rev. B **106**, 134509 (2022).

[34] Y. Song, J. Bi, Y. Nakamoto, K. Shimizu, H. Liu, B. Zou, G. Liu, H. Wang, and Y. Ma, Stoichiometric ternary superhydride $LaBeH_8$ as a new template for high-temperature superconductivity at 110 K under 80 GPa, Phys. Rev. Lett. **130**, 266001 (2023).

[35] K. Gao, W. Cui, J. Shi, A. P. Durajski, J. Hao, S. Botti, M. A. L. Marques, and Y. Li, Prediction of high-T_c superconductivity in ternary actinium beryllium hydrides at low pressure, Phys. Rev. B **109**, 014501 (2024).

[36] M. Gao, X.-W. Yan, Z.-Y. Lu, and T. Xiang, Phonon-mediated high-temperature superconductivity in the ternary borohydride KB_2H_8 under pressure near 12 GPa, Phys. Rev. B **104**, L100504 (2021).

[37] S. Li, H. Wang, W. Sun, C. Lu, and F. Peng, Superconductivity in compressed ternary alkaline boron hydrides, Phys. Rev. B **105**, 224107 (2022).

[38] A. Sanna, T. F. Cerqueira, Y.-W. Fang, I. Errea, A. Ludwig, and M. A. Marques, Prediction of ambient pressure conventional superconductivity above 80 K in hydride compounds, npj Comput. Mater. **10**, 44 (2024).

[39] K. Dolui, L. J. Conway, C. Heil, T. A. Strobel, R. P. Prasankumar, and C. J. Pickard, Feasible route to high-temperature ambient-pressure hydride superconductivity, Phys. Rev. Lett. **132**, 166001 (2024).

[40] X. Song, X. Hao, X. Wei, X.-L. He, H. Liu, L. Ma, G. Liu, H. Wang, J. Niu, S. Wang *et al.*, Superconductivity above 105 K in nonclathrate ternary lanthanum borohydride below megabar pressure, J. Am. Chem. Soc. **146**, 13797 (2024).

[41] D. V. Semenok, A. G. Kvashnin, I. A. Kruglov, and A. R. Oganov, Actinium hydrides AcH_{10}, AcH_{12}, and AcH_{16} as high-temperature conventional superconductors, J. Phys. Chem. Lett. **9**, 1920 (2018).

[42] C. Kokail, W. von der Linden, and L. Boeri, Prediction of high-T_c conventional superconductivity in the ternary lithium borohydride system, Phys. Rev. Mater. **1**, 074803 (2017).

[43] X. Du, S. Zhang, J. Lin, X. Zhang, A. Bergara, and G. Yang, Phase diagrams and electronic properties of BS and HBS systems under high pressure, Phys. Rev. B **100**, 134110 (2019).

[44] S. Di Cataldo, W. von der Linden, and L. Boeri, Phase diagram and superconductivity of calcium borohyrides at extreme pressures, Phys. Rev. B **102**, 014516 (2020).

[45] X. Li, X. Zhang, A. Bergara, Y. Liu, and G. Yang, Structural and electronic properties of Na-B-H compounds at high pressure, Phys. Rev. B **106**, 174104 (2022).

[46] W. Sukmas, P. Tsuppayakorn-aek, P. Pluengphon, S. J. Clark, R. Ahuja, T. Bovornratanaraks, and W. Luo, First-principles calculations on superconductivity and H-diffusion kinetics in Mg-B-H phases under pressures, Int. J. Hydrogen Energy **48**, 4006 (2023).

[47] Y. Wang, J. Lv, L. Zhu, and Y. Ma, Crystal structure prediction via particle-swarm optimization, Phys. Rev. B **82**, 094116 (2010).

[48] Y. Wang, J. Lv, L. Zhu, and Y. Ma, CALYPSO: A method for crystal structure prediction, Comput. Phys. Commun. **183**, 2063 (2012).

[49] B. Gao, P. Gao, S. Lu, J. Lv, Y. Wang, and Y. Ma, Interface structure prediction via CALYPSO method, Sci. Bull. **64**, 301 (2019).

[50] X. Shao, J. Lv, P. Liu, S. Shao, P. Gao, H. Liu, Y. Wang, and Y. Ma, A symmetry-orientated divide-and-conquer method for crystal structure prediction, J. Chem. Phys. **156**, 014105 (2022).

[51] K. Parlinski, Z. Q. Li, and Y. Kawazoe, First-principles determination of the soft mode in cubic ZrO_2, Phys. Rev. Lett. **78**, 4063 (1997).

[52] A. Togo, F. Oba, and I. Tanaka, First-principles calculations of the ferroelastic transition between rutile-type and $CaCl_2$-type SiO_2 at high pressures, Phys. Rev. B **78**, 134106 (2008).

[53] G. Kresse and J. Furthmüller, Efficient iterative schemes for *ab initio* total-energy calculations using a plane-wave basis set, Phys. Rev. B **54**, 11169 (1996).

[54] J. P. Perdew, K. Burke, and M. Ernzerhof, Generalized gradient approximation made simple, Phys. Rev. Lett. **77**, 3865 (1996).

[55] J. P. Perdew, J. A. Chevary, S. H. Vosko, K. A. Jackson, M. R. Pederson, D. J. Singh, and C. Fiolhais, Atoms, molecules, solids, and surfaces: Applications of the generalized gradient approximation for exchange and correlation, Phys. Rev. B **46**, 6671 (1992).

[56] G. Kresse and D. Joubert, From ultrasoft pseudopotentials to the projector augmented-wave method, Phys. Rev. B **59**, 1758 (1999).

[57] A. D. Becke and K. E. Edgecombe, A simple measure of electron localization in atomic and molecular systems, J. Chem. Phys. **92**, 5397 (1990).

[58] R. F. Bader, Atoms in molecules, Acc. Chem. Res. **18**, 9 (1985).

[59] P. Giannozzi, S. Baroni, N. Bonini, M. Calandra, R. Car, C. Cavazzoni, D. Ceresoli, G. L. Chiarotti, M. Cococcioni, I. Dabo *et al.*, QUANTUM ESPRESSO: a modular and open-source software project for quantum simulations of materials, J. Phys.: Condens. Matter **21**, 395502 (2009).

[60] See Supplemental Material at http://link.aps.org/supplemental/10.1103/PhysRevB.110.064105 for the charge transfer, the electronic properties and phonon dispersions of other compounds at different pressures, and structure information of all the compounds, etc.

[61] P. B. Allen and R. Dynes, Transition temperature of strong-coupled superconductors reanalyzed, Phys. Rev. B **12**, 905 (1975).

[62] Y. Yao and R. Hoffmann, BH_3 under pressure: Leaving the molecular diborane motif, J. Am. Chem. Soc. **133**, 21002 (2011).

[63] K. Abe and N. W. Ashcroft, Crystalline diborane at high pressures, Phys. Rev. B **84**, 104118 (2011).

[64] C.-H. Hu, A. R. Oganov, Q. Zhu, G.-R. Qian, G. Frapper, A. O. Lyakhov, and H.-Y. Zhou, Pressure-induced stabilization and insulator-superconductor transition of BH, Phys. Rev. Lett. **110**, 165504 (2013).

[65] A. Torabi, Y. Song, and V. N. Staroverov, Pressure-induced polymorphic transitions in crystalline diborane deduced by comparison of simulated and experimental vibrational spectra, J. Phys. Chem. C **117**, 2210 (2013).

[66] A. M. Murcia Rios, D. N. Komsa, and V. N. Staroverov, Effects of dispersion corrections and nonlocality on density functional predictions of pressure-induced polymorphic transitions of crystalline diborane, J. Phys. Chem. C **122**, 14781 (2018).

[67] W.-H. Yang, W.-C. Lu, S.-D. Li, X.-Y. Xue, Q.-J. Zang, K.-M. Ho, and C.-Z. Wang, Novel superconducting structures of BH_2 under high pressure, Phys. Chem. Chem. Phys. **21**, 5466 (2019).

[68] W.-H. Li, W.-H. Yang, and W.-C. Lu, Pressure-induced superconductivity of Ac-B-H hydrides, Phys. Chem. Chem. Phys. **25**, 22032 (2023).

[69] G. M. Eliashberg, Interactions between electrons and lattice vibrations in a superconductor, Sov. Phys. JETP **11**, 3 (1960).